

# Nanoscale

Accepted Manuscript



This is an *Accepted Manuscript*, which has been through the Royal Society of Chemistry peer review process and has been accepted for publication.

*Accepted Manuscripts* are published online shortly after acceptance, before technical editing, formatting and proof reading. Using this free service, authors can make their results available to the community, in citable form, before we publish the edited article. We will replace this *Accepted Manuscript* with the edited and formatted *Advance Article* as soon as it is available.

You can find more information about *Accepted Manuscripts* in the [Information for Authors](#).

Please note that technical editing may introduce minor changes to the text and/or graphics, which may alter content. The journal's standard [Terms & Conditions](#) and the [Ethical guidelines](#) still apply. In no event shall the Royal Society of Chemistry be held responsible for any errors or omissions in this *Accepted Manuscript* or any consequences arising from the use of any information it contains.

# Single nickel-related defects in molecular-sized nanodiamonds for multicolor bioimaging: an ab-initio study

Gergő Thiering\*    Elisa Londero†    Adam Gali‡

July 18, 2014

## Abstract

Fluorescent nanodiamonds constitute an outstanding alternative to semiconductor quantum dots and dye molecules for *in-vivo* biomarker applications where the fluorescence comes from optically active point defects acting as color centers in nanodiamonds. For practical purposes, these color centers are required to be photostable as a function of laser power or the surface of nanodiamonds and to exhibit a sharp and nearly temperature-independent zero-phonon line. In this study, we show by hybrid density-functional-theory calculations that nickel doped nanodiamonds exhibit the desired properties, opening thus the avenue to practical applications. In particular, harnessing the strong quantum confinement effect in molecular-sized nanodiamonds is very promising for achieving multicolor imaging by single nickel-related defects.

---

\*Wigner Research Centre for Physics and Optics, Hungarian Academy of Sciences, P.O. Box 49, H-1525 Budapest, Hungary

†Wigner Research Centre for Physics and Optics, Hungarian Academy of Sciences, P.O. Box 49, H-1525 Budapest, Hungary

‡Wigner Research Centre for Physics and Optics, Hungarian Academy of Sciences, P.O. Box 49, H-1525 Budapest, Hungary & Department of Atomic Physics, Budapest University of Technology and Economics, Budafokiút 8., H-1111 Budapest, Hungary

## 1 Introduction

Biologically compatible markers are much sought-after for the study of processes in living cells by means of *in vivo* multicolor imaging. Their action consists of binding to nanosized objects and tracking their location by emitting light upon excitation. To this end, semiconductor quantum dots and dye molecules have been used in the recent past.<sup>1,2</sup> The former bring the advantages of having small size, high photo-stability and bright multicolor fluorescence while on the other side they are toxic. Reduction of cytotoxicity is achieved by encapsulation which leads to a change in their photophysical properties and to a consequent growth in size after surface modification. Dye molecules on the other hand lack of photostability, presenting blinking and photobleaching at room temperature (see ref.<sup>3</sup> and references therein). This constitutes a major problem when long-term and repetitive monitoring of the bioactive compound is wanted. To solve this problem, a promising strategy to embed photo-stable color centers into bioinert nanocrystals<sup>3,4</sup> such as nanodiamonds.<sup>5</sup> Small diamond cages or nanodiamonds are obvious choice for *in vivo* bioimaging as they (i) contain bioinert carbon atoms, (ii) show low chemical reactivity,<sup>6</sup> (iii) and traditional organo-chemistry may be applied for surface functionalization.<sup>7</sup> However, diamond has an ultra-violet band gap. In ultra-small nanodiamonds the band gap is enlarged due to quantum confinement, thus pure nanodiamonds with clean surface are not fluorescent. It is important to mention here that their highest occupied molecular orbital (HOMO) indeed exhibit the quantum confinement effect whereas their lowest unoccupied molecular orbital (LUMO) is often surface related and weakly dependent on the size of the nanodiamonds; for instance, it is a weakly bound Rydberg-like state in hydrogenated nanodiamonds.<sup>8</sup> Visible or longer wave lengths emission can only be achieved by introducing color centers into nanodiamonds. The famous nitrogen-vacancy defect (NV) is such a color center in diamond, with unique properties and measurement abilities when its photoluminescence (PL) combined with magnetic resonance techniques.<sup>5</sup> NV-center has a large phonon-side band,<sup>9</sup> however, it is desirable to embed such color centers in bioimaging applications that have sharp zero-phonon lines in order to achieve the suf-

ficient contrast for multicolor imaging. Moreover, according to calculations,<sup>10</sup> the NV center has shown to be not stable in ultra-small nanodiamonds. Alternative optically active point defects with favorable properties in ultrasmall nanodiamonds are highly required for *in vivo* bioimaging applications. Recently, it has been demonstrated in meteorite nanodiamonds that fluorescent Si-V center can be stable in molecular-sized nanodiamonds,<sup>11</sup> where we were able to characterize this center with our simulation tools, showing relatively small quantum confinement effect. Here, we take one step further by characterizing nickel-related defects in nanodiamonds.

In this paper we show by advanced hybrid density-functional-theory (DFT) calculations that fluorescent nickel-related defects with sharp emission are stable in ultra-small nanodiamonds. Their excitations are calculated with time-dependent DFT. In molecule-sized nanodiamonds the wave length of the emission from the nickel-related color centers show *strong quantum confinement*, thus tight control of the size of nanodiamonds makes possible to realize multicolor bioimaging with single nickel-related defects, in contrast to the traditional and technologically challenging way of introducing multiple color centers. These color centers are paramagnetic in the ground state, which provides the opportunity to trace these nanoparticles both by light and magnetic fields at the same time.

Nanoparticle geometries were constructed by cutting approximately spherical clusters out of bulk diamond crystal, with varying diameter in the 1.1-2.0 nm range: C<sub>147</sub> ( $d=1.1$  nm), C<sub>175</sub> ( $d=1.2$  nm), C<sub>375</sub> ( $d=1.55$  nm), C<sub>452</sub> ( $d=1.7$  nm), and C<sub>633</sub> ( $d=1.9$  nm). We applied a standard methodology to terminate the surface of nanodiamonds: the surface dangling bonds were passivated by hydrogen atoms. We note that hydrogenated nanodiamonds may be achieved by hydrogen plasma treatment.<sup>12,13</sup> These nanodiamonds are considered as pristine ones. Pristine nanodiamonds possess excitation energies in the ultraviolet region. In order to introduce redshift in the excitation spectrum of nanodiamonds we placed nickel-related defects that may act as color centers. Particularly, we considered the so-called NE4\*,<sup>14</sup> NE4<sup>15,16</sup> and NE8<sup>17</sup> electron paramagnetic resonance (EPR) centers that are associated with the 1.83 eV (678 nm),<sup>14</sup> 1.72 eV (721 nm),<sup>18</sup> and 1.56 eV (794 nm)<sup>17</sup> PL centers in bulk diamond, respectively. Re-

cently, the NE4\* and NE4 centers were associated with different charge states of VNiV defects,<sup>19,20</sup> where VNiV represents a split-vacancy configuration (see Fig. 5). This defect is more stable than the isolated substitutional nickel-defect (W8 EPR center).<sup>19–21</sup> In addition, W8 defect is rather an absorption than a luminescence center in diamond according to our recent calculation,<sup>22</sup> thus we excluded it in this study. The NE8 defect is associated with a complex of four nitrogen atoms around the split VNiV defect (see Fig. 6), briefly, N<sub>2</sub>VNiVN<sub>2</sub> complex,<sup>17,20</sup> where the defect might be positively charged under typical measurement conditions. As shown above, nickel-related defects with sharp zero-phonon-lines in their PL spectra might be the best understood transition metal impurity related defects in bulk diamond. Furthermore, NE8 PL center can act as a bright single photon source at NIR region in bulk diamond,<sup>23,24</sup> thus it is particularly attractive color center for bioimaging. We note that NE8 defect could be engineered into diamond grains where their average diameter were between 30 and 100 nm.<sup>25</sup> The corresponding PL spectra did not differ from those obtained in bulk diamond because no quantum confinement takes place. However, quantum confinement might provide sizable effect on the optical properties of nickel-related defects in small nanodiamonds.

We studied the optical properties of NE4\*, NE4 and NE8 color centers in small nanodiamonds by time-dependent density functional theory calculations (TD-DFT) with using hybrid functional in its kernel where this methodology was proven to provide reliable results for nanodiamonds with different surface terminations,<sup>8,26</sup> including color centers inside hydrogenated nanodiamonds.<sup>11,27</sup> NE4 and NE8 defects may be considered as nickel-related color centers in nitrogen-free and highly nitrogen-contaminated nanodiamonds. We note that the experimental Stokes-shift of the considered PL centers is about 30 meV<sup>17</sup> which is smaller than the expected accuracy of our method, thus we calculated the excitation energies at the ground state geometry of the defects. For bulk reference calculations we applied such a hybrid DFT supercell plane wave methodology that is able to reproduce the experimental defect ionization energies within 0.1 eV in Group-IV semiconductors,<sup>28,29</sup> and is proven to be correct for substitutional Ni impurity (Ni<sub>s</sub>) in diamond.<sup>22</sup>

## 2 Results and discussion

We computed the electronic levels and the lowest excitation energies of the selected nanodiamonds that contained nickel defects. Fig. 1 shows the most important results of our work. We find that

- i) the introduction of color centers to the nanodiamonds redshifts their excitation energies from the ultraviolet region of pristine nanodiamonds.
- ii) Quantum confinement effect (QCE) is very strong on the defect levels in the gap of nanodiamonds both for NE4 and NE8 color centers [Fig. 1(a)], and the highest energy occupied defect states significantly hybridized with the host diamond states.
- iii) As a consequence, strong QCE arises in the luminescence of these color centers [Fig. 1(c)]. We propose that single VNiV defects in nitrogen-free nanodiamonds and single N<sub>2</sub>VNiVN<sub>2</sub> defects in highly nitrogen-contaminated nanodiamonds may be utilized to realize multicolor imaging in the visible toward the infrared region by fine controlling the size of nanodiamonds. Small nanodiamonds hosting these nickel color centers would provide an ideal platform for non-invasive *in vivo* bioimaging. Next, we discuss the stability of the defect in hydrogenated nanodiamonds and bulk diamond, the photo-stability of these color centers in hydrogenated nanodiamonds. Finally, we analyze the nature of the excitation and we provide the reason for the strong quantum confinement effect.

First, we studied the stability of the selected nickel defects by calculating the formation energies of the defects in nanosized and bulk diamonds as plotted in Fig. 2(a) when the defect is placed in the middle of the nanodiamonds. The VNiV defect is about equally stable in bulk and molecule-sized diamonds. Surprisingly, the N<sub>2</sub>VNiVN<sub>2</sub> is even more stable in molecule-sized nanodiamonds than in bulk diamond. These results indicate that once these defects were created in nanodiamonds they will remain there. Next, we considered the relative stability of the corresponding color centers as a function of their position in our largest 1.9-nm nanodiamond [Fig. 2(b)-(d)]. We assumed that the first neighbor shell around the defect should contain carbon atoms when they approach the surface. For both defects relatively small fluctuations in the calculated

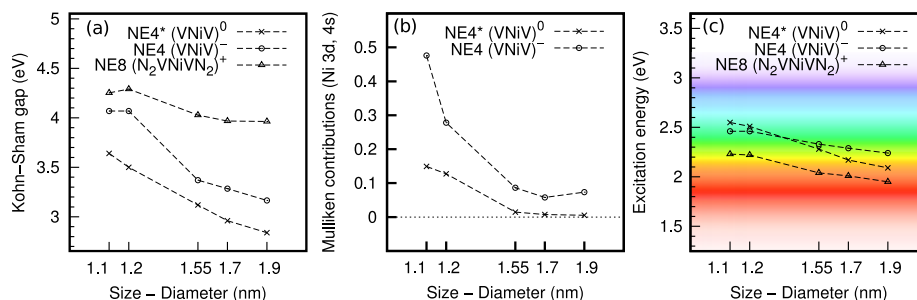


Figure 1: (a) Weighted Kohn-Sham gap of the defects as a function of the size of the hydrogenated nanodiamonds as calculated by spin-polarized PBE0 hybrid density functional theory. The weights of pairs of Kohn-Sham states were determined from time-dependent density functional theory calculations as the contribution of these pairs of Kohn-Sham states to the first excitation peak. (b) Contribution of the nickel orbitals in the occupied Kohn-Sham states that participate in the lowest-energy excitation as a function of the size of the hydrogenated nanodiamonds determined by Mulliken analysis. Note the large reduction of this contribution for NE4 center which manifests as smoother slope of the excitation energy as a function of the size of the hydrogenated nanodiamonds. (c) The calculated excitation energies of the corresponding color centers are plotted as a function of the size of the nanodiamonds.

formation energies can be observed. Apparently, no thermodynamic force appears to drive these color centers toward the edge of nanodiamonds. We conclude that these color centers may be found in molecule-sized nanodiamonds once they formed.

Next, we studied the photo-stability of the Ni-related color centers from the aspect of surface termination. It is well-known from the studies of NV-center that NV-center can switch its charge state from negative to neutral when NV-center is close to the hydrogenated diamond surface<sup>30-32</sup> which is explained by the band bending model between the diamond surface and the environment.<sup>33</sup> Particularly, it is expected that NV defect can be predominantly found in its neutral charge state in hydrogenated nanodiamond.<sup>34</sup> We use the charge transition levels of NV defect in bulk diamond as a marker to determine whether the selected Ni-related color centers are stable in their given charge states in hydrogenated nanodiamonds. For the sake of completeness, we also include Ni<sub>s</sub> defect in this study<sup>22</sup> but we focus on the VNiv and N<sub>2</sub>VNiVN<sub>2</sub> complexes. The results are plotted in Fig. 3. There is a window of the Fermi-level positions where NV is stable in its neutral charge state in bulk diamond. In this window the VNiv defect can be neutral, negatively charged and double negatively charged. Its cal-

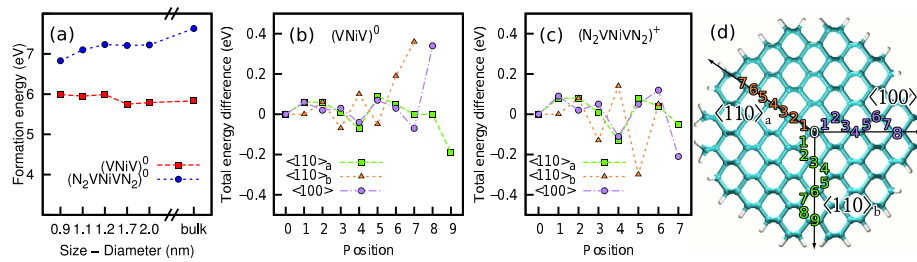


Figure 2: Stability of nickel-related defects in different diamonds calculated at DFT PBE level. (a) The calculated formation energies of the selected defects as a function of the size of the diamonds. The defects were placed in the middle of the nanodiamonds. (b) and (c) shows the relative stability of VNiV and N<sub>2</sub>VNiVN<sub>2</sub> color centers within 1.9-nm hydrogenated nanodiamonds as a function of their position. (d) shows 1.9-nm hydrogenated nanodiamond with labeling the positions where we placed the Ni impurity of the selected defects within the nanodiamonds. Because of the lack of inversion symmetry within the nanodiamonds the depicted  $\langle 110 \rangle_a$  and  $\langle 110 \rangle_b$  directions are not equivalent.

culated  $(-|2-)$  charge transition level is at around  $E_V+2.0$  eV, where  $E_V$  is the valence band edge. This is about 0.7 eV below the  $(0|-)$  charge transition level of NV defect. No visible luminescence is expected from VNiV defect in  $(2-)$  charge state but its  $(-)$  and  $(0)$  charge states should show luminescence. We conclude that VNiV-related luminescence is expected in hydrogenated nanodiamonds and might be not detected in oxygenated or fluorinated nanodiamonds<sup>34–36</sup> where the Fermi-level shifts higher with stabilizing the NV<sup>-</sup> defect. Since the calculated  $(0|-)$  charge transition level of VNiV lies relatively deep in the gap at around  $E_V+1.2$  eV, it is more likely that NE4 center will be active in hydrogenated nanodiamonds. The situation is more simple for the N<sub>2</sub>VNiVN<sub>2</sub> complex. The defect is mostly stable in its  $(+)$  charge state as a function of the position of Fermi-level in diamonds, particularly, in the full stability window of NV<sup>0</sup>. We note that neutral N<sub>2</sub>VNiVN<sub>2</sub> has  $S = 1$  ground state. The calculated  $(+|0)$  charge transition level is at around  $E_V+2.9$  eV which is 0.2 eV above the  $(0|-)$  charge transition level of NV defect. This result indicates that NE8 color center should have a stable luminescence in hydrogenated nanodiamond, and it may emit light even in oxygenated nanodiamonds where NV<sup>-</sup> is stabilized. Thus, NE8 color center embedded in hydrogenated nanodiamonds is ideal to ensure stable luminescence.

It is imperative to analyze the electronic structure of the selected Ni-related color

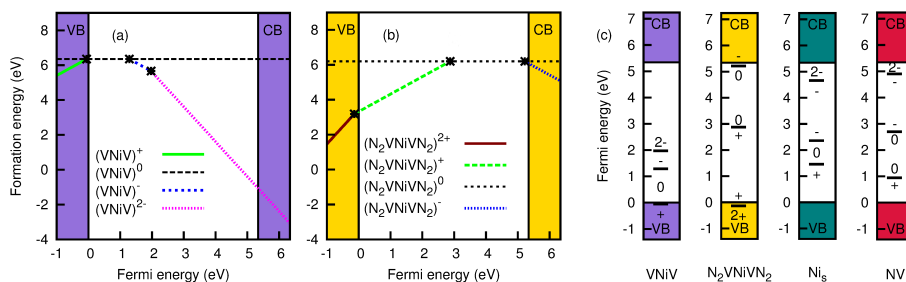


Figure 3: The calculated formation energies and charge transition levels in bulk diamond at DFT HSE06 level. (a) and (b) plots the formation energies for VNiv and N<sub>2</sub>VNiVN<sub>2</sub> defects, respectively, as a function of the position of Fermi-level in the band gap of diamond. The calculated valence band edge was aligned to the origo. The valence band (VB) and conduction band (CB) edges are also depicted by shaded areas where the color of these areas corresponds to color code of the given defects in (c). The charge transition levels can be read as the crossings between the lines. (c) Charge transition levels in the band gap are depicted for the given defects where the Ni<sub>s</sub> and NV levels were given in Refs.<sup>22,29</sup>

centers in order to understand the nature of their optical transition and the strong quantum confinement effect on their excitation energies in nanodiamonds. We start the analysis with the split-vacancy VNiv defect which might be described by substituting a divacancy (two adjacent vacancies in diamond) with a single Ni impurity where this impurity is placed in halfway between the two vacant sites. Thus, Ni atom lies in the inversion center of the diamond lattice. The electronic structure of this system was already studied in previous papers,<sup>19,20</sup> thus we only provide a brief description by applying the powerful group theory with the combination of DFT HSE06 calculations in bulk diamond. The full system has  $D_{3d}$  symmetry. Six dangling bonds create  $a_{2u}^{(2)} a_{1g}^{(2)} e_g^{(2)} e_u^{(0)}$  states. The Ni 3d orbitals split in this crystal field as  $a_{1g}^{(2)} e_g^{(4)} e_g^{(4)}$ . The  $a_{1g}$  and  $e_g$  states can principally hybridize whereas the  $a_{2u}$  and  $e_u$  vacancy-like states will be exclusively localized on the carbon dangling bonds of the divacancy (see Fig. 5). The former lies deep in the valence band whereas the latter has higher energy. Between the two levels can be found the  $e_g$  and  $a_{1g}$  molecule-like levels except one antibonding combination of the  $e_g$  state which is empty and lies high in the band gap of diamond. The resulted states of neutral VNiv defect may be described as  $a_{2u}^{(2)} a_{1g}^{(2)} e_g^{(4)} a_{1g}^{(2)} e_g^{(4)} e_u^{(2)} e_g^{(0)}$ . The  $a_{2u}$  and the empty  $e_g$  states do not play a role in the lowest energy excitations. By spin-polarized

DFT HSE06 calculations we found in bulk diamond that the fully occupied spin-up  $e_u$  state is resonant with the valence band whereas the spin-down empty  $e_u$  state appears clearly in the band gap with building up a high spin  $S = 1$  state (c.f., Fig. 4). This qualitatively agrees with a previous DFT PBE supercell calculation.<sup>20</sup> Excitation may occur from the resonant spin-down  $a_{1g}$  or  $e_g$  states to the empty  $e_u$  state that is optically allowed by parity. In  $\text{VNiV}^-$  defect the  $e_u$  state is occupied by three electrons which is principally Jahn-Teller unstable system. Nevertheless, the Jahn-Teller distortion is small in agreement with the previous findings.<sup>20</sup> The DFT HSE06 method predict  $C_{2h}$  symmetry of the system which slightly splits the degenerate  $e_u$  and  $e_g$  states to  $a_u \oplus b_u$  and  $a_g \oplus b_g$  states, respectively. The corresponding defect levels shift up with respect to the defect levels of  $\text{VNiV}^0$  (c.f., Fig. 4) in agreement with the previous finding.<sup>20</sup> The excitation may be expected again from the occupied resonant  $a_g$  and  $b_g$  states to the empty  $a_u$  state. In  $\text{N}_2\text{VNiVN}_2$  complex four carbon atoms around Ni impurity are substituted by nitrogen atoms, so the defect has *per se*  $C_{2h}$  symmetry. The four nitrogen atoms provide four extra electrons to the system with respect to the  $\text{VNiV}$  defect. The resulting electronic structure is shown in Figs. 4, 6. In the positive charge state of the defect the  $b_u$  level is fully occupied, and the unpaired spin will be localized on the  $b_g$  level with resulting in  $S = 1/2$  spin state. The  $b_u$  state is resonant with the valence band whereas the empty  $a_g$  state can be found in the band gap of bulk diamond. Excitation may be expected between the  $b_u$  and  $a_g$  states. The excitations of these defects were investigated in nanodiamonds.

In nanodiamonds the inversion symmetry is broken, strictly speaking. Thus,  $D_{3d}$  reduces to  $C_{3v}$  whereas  $C_{2h}$  to  $C_{1h}$  symmetries going from bulk diamond to nanodiamond. However, the corresponding defect states still resemble the character of such wave functions that have parity (see Figs. 5, 6). We conclude that it is reasonable to apply the selection rules of assuming inversion center in the defects and to label the corresponding defect states by the symmetry group associated with the defects in bulk diamond.

In  $\text{VNiV}^0$  defect, the excitation occurs from the  $e_g$  and  $a_{1g}$  states to the  $e_u$  state. The  $e_u$  state is clearly gap and shows relatively small quantum confinement effect. How-

ever, the  $e_g$  and  $a_{1g}$  states appears in the "valence" band of the host nanodiamond. In the smallest nanodiamonds, the localization on Ni-atom can be observed, however, at larger nanodiamonds the contribution becomes weaker and several resonant states appear at deeper energies [see Fig. 1(b)]. In bulk diamond, these states becomes almost completely delocalized [see Figs. 4(b,c)]. These states show strong quantum confinement (similar to that of the host nanodiamond "valence band maximum" states) which results in relatively strong quantum confinement on the excitation energy.

In  $\text{VNiV}^-$  defect, the electronic structure is more complex. As mentioned for the bulk case, the double degenerate  $e_u$  state is occupied by three electrons which is a subject of Jahn-Teller distortion resulting in  $C_{2h}$  symmetry. The  $e_u$  state splits to  $a_u$  and  $b_u$  where the hole may reside either on  $a_u$  or  $b_u$  state which lead to different type of distortion. According to our calculations, the energy difference between the two possible distortions are within 0.1 eV in nanodiamonds. We always chose the lowest energy configurations in the calculation of excitation. The hole resides on the  $b_u$  state in the lowest energy configurations in most of the considered nanodiamonds except the largest one where the hole is found on the  $a_u$  state. Interestingly, in bulk diamond HSE06 calculations also predict the hole on the  $a_u$  state. Generally, the defect levels shift up with respect to the case of neutral defect. As a consequence, the  $a_{1g}$  and the split  $e_g$  states get strongly localized on the Ni-atom (and around the defect) in the smallest nanodiamonds of  $d=1.1-1.2$  nm. In larger nanodiamonds, these states starts to smear in the "valence band", and the character of these wave functions changes significantly [see Fig. 1(b)]. This issue has serious consequence in the excitation energies. Despite the Kohn-Sham gaps significantly drop going from  $d=1.1-1.2$  nm to larger nanodiamonds, the excitation energies do not follow this trend. When all the defect states are localized participating in the excitation then the electron-hole attractive interaction is about 1.8 eV. This electron-hole interaction is weaker (about 1.0 eV) when the hole part gets delocalized in the excited state. This effect is much less visible for the neutral defect where the  $a_{1g}$  and  $e_g$  states are *per se* less localized in the smallest nanodiamonds.

Finally, the  $\text{N}_2\text{VNiVN}_2^+$  defect is briefly analyzed. In this case, the  $b_u$  state can be found in the band gap of the considered nanodiamonds but its quantum confinement is

less pronounced than that of the "valence band maximum" states. As a consequence, this  $b_u$  state becomes resonant in bulk diamond. Because both the hole and electron parts of the exciton state are localized the electron-hole interaction is about 2.0 eV, almost independently from the size of the nanodiamond. The quantum confinement on the excitation energies of this defect is weaker than for VNiV defect but still considerable and allows multi-color imaging from yellow down to infrared as a function of the size of the nanodiamonds.

### 3 Conclusions

In summary, we have calculated the lowest excitation energy of nickel-related defects in hydrogenated nanodiamonds with assuming large concentration of nitrogen and no nitrogen. We found that the excitation energy depends very significantly on the size of the nanodiamonds because the transition occurs between a heavily perturbed valence band like state which is a subject of quantum confinement. We propose that multi-color *in vivo* bioimaging agents can be fabricated with these single color centers in molecule-sized nanodiamonds when the size of the nanodiamonds can be fine controlled. All of the considered color centers are paramagnetic that gives an additional freedom for sensing.

### 4 Computational methods

We modeled the defects in bulk diamond by supercell method. We used 512-atom simple cubic supercell where the Brillouin zone of the supercell was sampled at the  $\Gamma$ -point. This method provides sufficiently convergent charge density and the degeneracy of the defect states can be monitored accordingly. We applied a screened, range-separated, non-local hybrid density functional theory (DFT), called HSE06,<sup>37,38</sup> to calculate the electronic structure and the geometry of the defects. The optimal positions of the atoms are found by minimizing the Hellmann-Feynman forces until the remaining force on each of the atoms is less than 0.02 eV/Å. The projector-augmented wave

(PAW) method<sup>39</sup> together with plane wave basis set was utilized to calculate the charge and spin densities of the system as implemented in the VASP 5.3 code.<sup>40,41</sup> Within this framework, we chose to consider both the 3p and 3d Ni electrons as part of the valence. The energy cut-off for the expansion of the valence wave functions was set to 420 eV which is convergent for the charge densities of the system. We aligned the valence band edge to the perfect diamond in defective supercells and applied the 2/3 of the monopole term of the Makov-Payne charge correction<sup>42</sup> in charged defective supercells. This methodology is able to reproduce the experimental ionization energies within 0.1 eV for deep defects in Group-IV semiconductors.<sup>28,29</sup> We note that the presence of d-orbitals in  $sp^3$  electron bath of the host may represent a problem on the validity of HSE06 functional where extra correction on the functional may be needed.<sup>43</sup> By following the recipe in Ref.<sup>43</sup> to check the validity of the applied functional we found that HSE06 DFT functional gives accurate and trustworthy results for the VN<sub>i</sub>V and N<sub>2</sub>VN<sub>i</sub>VN<sub>2</sub> defects. This is in line with our previous finding on Ni<sub>s</sub> defect in diamond.<sup>22</sup>

The adiabatic charge transition levels (also called occupation levels) of the defects were calculated by the standard methodology (see<sup>28</sup> and references therein) by using the formation energy of the defect ( $E_{\text{form}}^Q$ ) with a given charge ( $Q$ ),

$$E_{\text{form}}^Q = E_{\text{tot}}^Q - \sum_i n_i \mu_i + q(E_F + E_V + \Delta V) + \Delta E_{\text{corr}}, \quad (1)$$

where  $\mu_i$  is the chemical potential of the element  $i$  with number of  $n_i$  in the supercell.  $\Delta V$  and  $\Delta E_{\text{corr}}$  are the potential alignment and correction of the charged supercell as explained above. We used the total energy of bulk diamond and nickel crystal to obtain the chemical potential of carbon and nickel, whereas the total energy of nitrogen molecule (simulated in a  $10^3 \text{ \AA}^3$  empty box) was used to obtain the chemical potential of nitrogen. In the symmetry analysis of the single particle defect states we applied projected density of states with using the standard projectors of PAW method.

We carried out *ab initio* calculations on nanodiamonds with diameter ( $d$ ) of 1 to 2 nm. The geometry optimizations were carried out within supercell formalism by us-

ing the Perdew-Burke-Ernzerhof (PBE)<sup>44</sup> within DFT. We used a 420 eV and 1260 eV cutoff for the wavefunction and charge density expansions, respectively. We applied standard PAW-potentials for the ions as implemented in the VASP code. The geometry of the nanodiamonds were optimized until all forces fell below 0.01 eV/Å. The distance between any surface atoms of the periodic images was larger than 1 nm, thus the interaction between the nanodiamonds was negligible. We calculated the formation energies of the defects in the nanodiamond at DFT PBE level by modifying Eq. 1,

$$E_{\text{form}} = E_{\text{tot}} - E_{\text{tot}}^{\text{pristine}} - \sum_i \Delta n_i \mu_i, \quad (2)$$

where  $E_{\text{tot}}^{\text{pristine}}$  is the total energy of the pristine nanodiamond, and  $\Delta n_i$  is the number of  $i$ -type of atoms in the defective nanodiamond with respect to the number of those atoms in the pristine nanodiamond.

Excitation spectra were calculated by time-dependent density functional (TD-DFT) calculations by using TURBOMOLE cluster code<sup>45</sup> where the geometry of SiC QDs were taken from VASP calculations. We used double- $\zeta$  polarized basis set with eliminating the core electrons by effective core potentials, which allowed us to compute the excitation energies even for large nanodiamonds of  $d=1.9$  nm with 633 carbon atoms and 300 hydrogen atoms. We checked the convergence of the localized basis set by comparing the Kohn-Sham energies obtained with the plane-wave VASP code and the TURBOMOLE cluster code with PBE functional. The difference between the single particle gaps were smaller than 0.05 eV in each case. We applied PBE0 hybrid functional<sup>46</sup> in the TD-DFT kernel that provided reliable excitation energies for similar systems.<sup>8,11,26,27</sup>

## 5 Acknowledgements

The authors acknowledge the EU FP7 grant DIAMANT (grant no. 270197). AG acknowledges the support from the Lendület program of the Hungarian Academy of Sciences.

## References

- [1] X. Michalet, F. F. Pinaud, L. A. Bentolila, J. M. Tsay, S. Doose, J. J. Li, G. Sundaresan, A. M. Wu, S. S. Gambhir and S. Weiss, *Science*, 2005, **307**, 538–544.
- [2] J. Lippincott-Schwartz and G. H. Patterson, *Science*, 2003, **300**, 87–91.
- [3] B. Somogyi and A. Gali, *Journal of Physics: Condensed Matter*, 2014, **26**, 143202.
- [4] B. Somogyi, V. Zólyomi and A. Gali, *Nanoscale*, 2012, **4**, 7720–7726.
- [5] V. N. Mochalin, O. Shenderova, D. Ho and Y. Gogotsi, *Nat Nano*, 2012, **7**, 11–23.
- [6] A. M. Schrand, H. Huang, C. Carlson, J. J. Schlager, E. Osawa, S. M. Hussain and L. Dai, *The Journal of Physical Chemistry B*, 2007, **111**, 2–7.
- [7] J. Cheng, J. He, C. Li and Y. Yang, *Chemistry of Materials*, 2008, **20**, 4224–4230.
- [8] M. Vörös and A. Gali, *Physical Review B*, 2009, **80**, 161411.
- [9] G. Davies and M. Hamer, *Proceedings of the Royal Society of London. A. Mathematical and Physical Sciences*, 1976, **348**, 285–298.
- [10] C. Bradac, T. Gaebel, N. Naidoo, J. R. Rabeau and A. S. Barnard, *Nano Letters*, 2009, **9**, 3555–3564.
- [11] I. I. Vlasov, A. A. Shiryaev, T. Rendler, S. Steinert, S.-Y. Lee, D. Antonov, M. Vörös, F. Jelezko, A. V. Fisenko, L. F. Semjonova, J. Biskupek, U. Kaiser, O. I. Lebedev, I. Sildos, P. R. Hemmer, V. I. Konov, A. Gali and J. Wrachtrup, *Nature Nanotechn.*, 2014, **9**, 54–58.
- [12] H. Girard, J. Arnault, S. Perruchas, S. Saada, T. Gacoin, J.-P. Boilot and P. Bergonzo, *Diamond and Related Materials*, 2010, **19**, 1117 – 1123.
- [13] H. Girard, T. Petit, S. Perruchas, T. Gacoin, C. Gesset, J. Arnault and P. Bergonzo, *Physical Chemistry Chemical Physics*, 2011, **13**, 11517–11523.

- [14] K. Iakoubovskii, A. Stesmans, B. Nouwen and G. J. Adriaenssens, *Phys. Rev. B*, 2000, **62**, 16587–16594.
- [15] V. Nadolinny and A. Yelisseyev, *Diamond and Related Materials*, 1994, **3**, 1196 – 1200.
- [16] W. Gehlhoff and R. N. Pereira, *Journal of Physics: Condensed Matter*, 2002, **14**, 13751.
- [17] V. A. Nadolinny, A. P. Yelisseyev, J. M. Baker, M. E. Newton, D. J. Twitchen, S. C. Lawson, O. P. Yuryeva and B. N. Feigelson, *Journal of Physics: Condensed Matter*, 1999, **11**, 7357.
- [18] T. Pawlik, C. Noble and J.-M. Spaeth, *Journal of Physics: Condensed Matter*, 1998, **10**, 9833.
- [19] J. Goss, P. Briddon, R. Jones and S. Öberg, *Journal of Physics: Condensed Matter*, 2004, **16**, 4567.
- [20] R. Larico, J. F. Justo, W. V. M. Machado and L. V. C. Assali, *Phys. Rev. B*, 2009, **79**, 115202.
- [21] J. Isoya, H. Kanda, J. R. Norris, J. Tang and M. K. Bowman, *Phys. Rev. B*, 1990, **41**, 3905–3913.
- [22] T. Chanier and A. Gali, *Phys. Rev. B*, 2013, **87**, 245206.
- [23] J. R. Rabeau, Y. L. Chin, S. Praver, F. Jelezko, T. Gaebel and J. Wrachtrup, *Applied Physics Letters*, 2005, **86**, 131926.
- [24] M. Wolfer, A. Kriele, O. A. Williams, H. Obloh, C.-C. Leancu and C. E. Nebel, *physica status solidi (a)*, 2009, **206**, 2012–2015.
- [25] E. Wu, J. R. Rabeau, G. Roger, F. Treussart, H. Zeng, P. Grangier, S. Praver and J.-F. Roch, *New Journal of Physics*, 2007, **9**, 434.
- [26] M. Vörös, T. Demjén, T. Szilvási and A. Gali, *Phys. Rev. Lett.*, 2012, **108**, 267401.

- [27] A. Gali, *physica status solidi (b)*, 2011, **248**, 1337–1346.
- [28] P. Deák, B. Aradi, T. Frauenheim, E. Janzén and A. Gali, *Phys. Rev. B*, 2010, **81**, 153203.
- [29] P. Deák, B. Aradi, M. Kaviani, T. Frauenheim and A. Gali, *Phys. Rev. B*, 2014, **89**, 075203.
- [30] K.-M. C. Fu, C. Santori, P. E. Barclay and R. G. Beausoleil, *Applied Physics Letters*, 2010, **96**, 121907.
- [31] L. Rondin, G. Dantelle, A. Slablab, F. Grosshans, F. Treussart, P. Bergonzo, S. Perruchas, T. Gacoin, M. Chaigneau, H.-C. Chang, V. Jacques and J.-F. Roch, *Phys. Rev. B*, 2010, **82**, 115449.
- [32] M. V. Hauf, B. Grotz, B. Naydenov, M. Dankerl, S. Pezzagna, J. Meijer, F. Jelezko, J. Wrachtrup, M. Stutzmann, F. Reinhard and J. A. Garrido, *Phys. Rev. B*, 2011, **83**, 081304.
- [33] B. Grotz, M. V. Hauf, M. Dankerl, B. Naydenov, S. Pezzagna, J. Meijer, F. Jelezko, J. Wrachtrup, M. Stutzmann, F. Reinhard *et al.*, *Nature Communications*, 2012, **3**, 729.
- [34] V. Petráková, A. Taylor, I. Kratochvílová, F. Fendrych, J. Vacík, J. Kučka, J. Štursa, P. Cíglér, M. Ledvina, A. Fišerová, P. Kneppo and M. Nesládek, *Advanced Functional Materials*, 2012, **22**, 812–819.
- [35] K. J. Rietwyk, S. L. Wong, L. Cao, K. M. O'Donnell, L. Ley, A. T. S. Wee and C. I. Pakes, *Applied Physics Letters*, 2013, **102**, 091604.
- [36] S. Cui and E. L. Hu, *Applied Physics Letters*, 2013, **103**, 051603.
- [37] J. Heyd, G. E. Scuseria and M. Ernzerhof, *The Journal of Chemical Physics*, 2003, **118**, 8207–8215.
- [38] A. V. Krukau, O. A. Vydrov, A. F. Izmaylov and G. E. Scuseria, *The Journal of Chemical Physics*, 2006, **125**, 224106.

- [39] P. E. Blöchl, *Phys. Rev. B*, 1994, **50**, 17953.
- [40] G. Kresse and J. Furthmüller, *Phys. Rev. B*, 1996, **54**, 11169.
- [41] G. Kresse and J. Furthmüller, *Comput. Mat. Sci.*, 1996, **6**, 15.
- [42] G. Makov and M. C. Payne, *Phys. Rev. B*, 1995, **51**, 4014–4022.
- [43] V. Ivády, I. A. Abrikosov, E. Jánzén and A. Gali, *Phys. Rev. B*, 2013, **87**, 205201.
- [44] J. P. Perdew, K. Burke and M. Ernzerhof, *Phys. Rev. Lett.*, 1996, **77**, 3865–3868.
- [45] R. Bauernschmitt and R. Ahlrichs, *Chem. Phys. Letters*, 1996, **256**, 454–464.
- [46] J. P. Perdew, M. Ernzerhof and K. Burke, *The Journal of Chemical Physics*, 1996, **105**, 9982–9985.

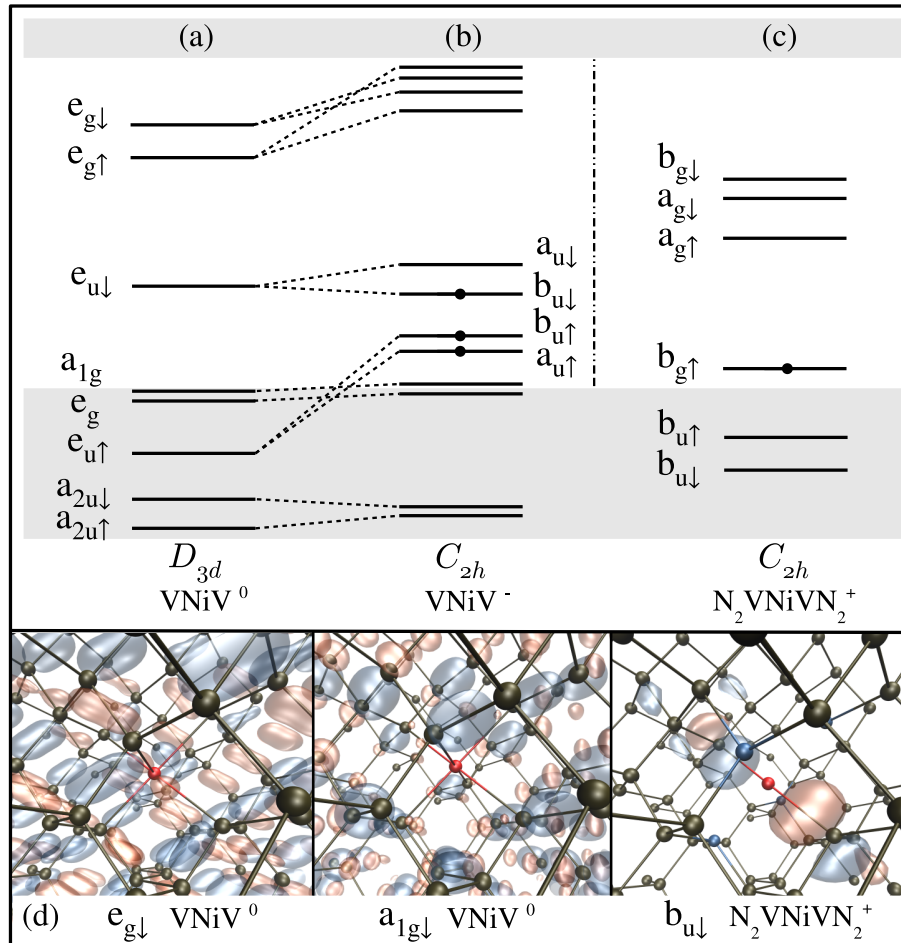


Figure 4: Schematic diagram about the DFT HSE06 single particle defect states with symmetry labels in bulk diamond for (a)  $\text{VNiV}^0$  (NE4\*), (b)  $\text{VNiV}^-$  (NE4), and (c)  $\text{N}_2\text{VNiVN}_2^+$  (NE8). The occupation of defect states in the gap is shown by dots. (d) Resonant defect states of  $\text{VNiV}^0$  and  $\text{N}_2\text{VNiVN}_2^+$  in bulk diamond. Absolute value of the isovalues of 0.022 and 0.1 were applied in  $\text{VNiV}^0$  and  $\text{N}_2\text{VNiVN}_2^+$  defects, respectively, where red(blue) lobes represents negative(positive) values of the corresponding wave functions. Strong hybridization between the  $e_g$  and  $a_{1g}$  resonant states and the host crystal states is apparent in  $\text{VNiV}^0$  defect. The resonant  $b_u$  state mixes much less with the host diamond states in  $\text{N}_2\text{VNiVN}_2^+$  defect.

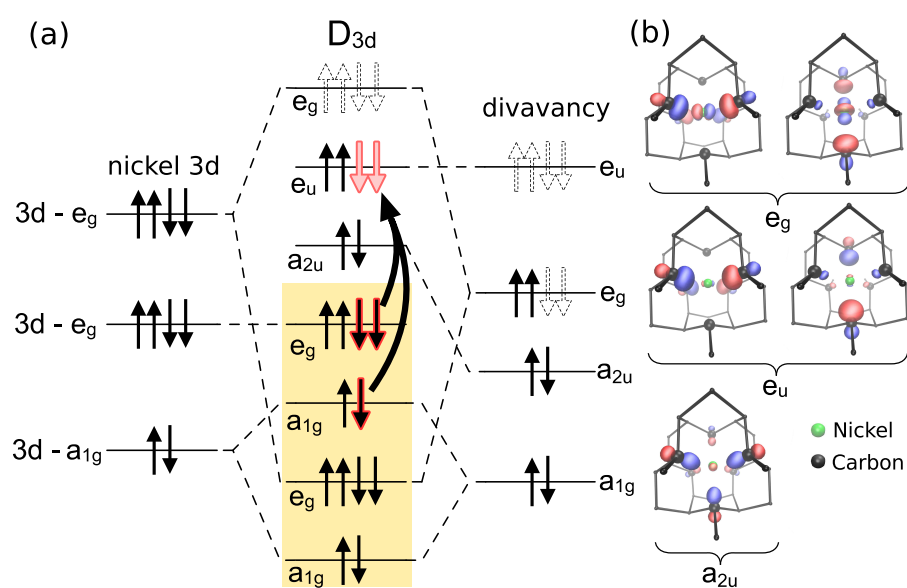


Figure 5: Group theory analysis of VNiV defect states in diamond. The wave functions and the Kohn-Sham levels are the result of the PBE0 calculation in the 1.1-nm nanodiamond. (a) Defect molecule diagram. The yellow background represents the valence band. The nature of the excitation in the neutral charge state (NE<sub>4</sub><sup>\*</sup>) is represented by arrows. (b) Single particle orbitals associated with the defect are represented by blue (positive) and red (negative) lobes with an absolute value of the isovalue of 0.065, where the defect is shown from the view of the symmetry axis.

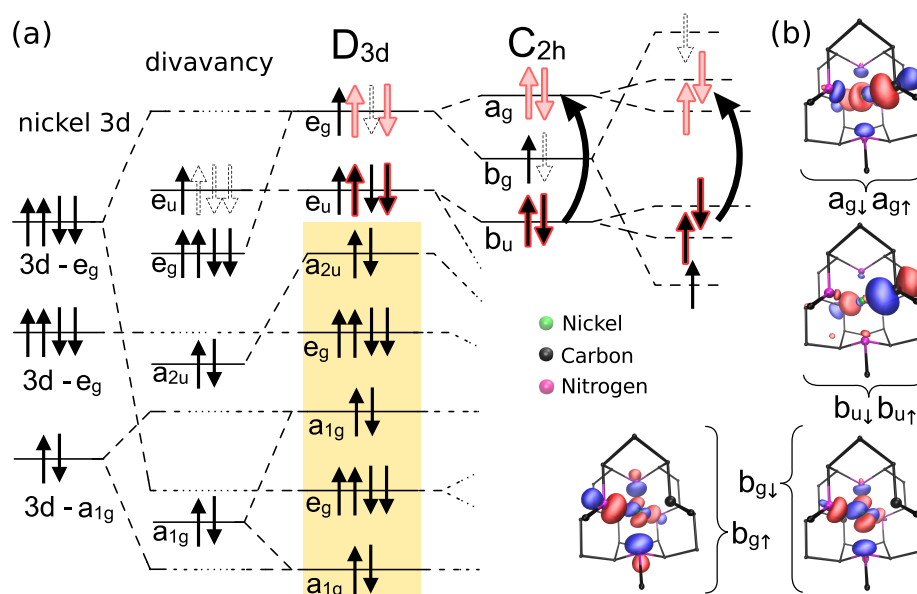


Figure 6: Group theory analysis of the  $N_2VNiVN_2$  in the positive charge state, the NE8 center. (a) Defect molecule diagram. The analysis start from left to right with that of  $VNiV$  states (c.f., Fig. 5) but with 4 extra electron donated by the 4 N-atoms. Next, we take into account that the crystal field is reduced from  $D_{3d}$  to  $C_{2h}$  due to the presence of N-atoms which splits the corresponding states. The final column shows that the large spin-polarization of  $b_g$  state, so the excitation occurs between  $b_u$  and  $a_g$  states. According to our time-dependent density functional theory calculations both spin states contribute to the excitation. (b) The wave functions and the Kohn-Sham levels are the result of the PBE0 calculation in the 1.1-nm nanodiamond. Single particle orbitals associated with the defect are represented by blue (positive) and red (negative) lobes with an absolute value of the isovalue of 0.065, where the defect is shown from the view of the symmetry axis.